



Multiparametric MRI combined with liver volume for quantitative evaluation of liver function in patients with cirrhosis

Chenxia Li* 
 Haitian Liu* 
 Jinhan Wang 
 Xiang Li 
 Ting Cui 
 Rong Wang 
 Jian Yang 
 Yuelang Zhang 

PURPOSE

We aimed to establish a liver function evaluation model by combining multiparametric magnetic resonance imaging (MRI) with liver volume (LV) and further verify the effectiveness of the model to evaluate liver function.

METHODS

This retrospective study included 101 consecutive cirrhosis patients (69 cases for modeling group and 32 cases for validation group) who underwent gadoxetic acid-enhanced MRI. Five signal intensity parameters were obtained by measuring the signal intensities of the liver, spleen, and erector spinae before and 20 minutes after gadoxetic acid disodium enhancement. The diffusion coefficient (D), pseudo-diffusion coefficient (D*), and perfusion fraction (f) were obtained from intravoxel incoherent motion diffusion-weighted imaging. The LV parameters ($V_{\text{liver}}/V_{\text{spleen}}$ and $V_{\text{liver}}/V_{\text{spleen}}$) were obtained using 3-dimensional image generation software. The most effective parameter was selected from each of the 3 methods, and a multivariate regression model for liver function evaluation was established and validated.

RESULTS

In the modeling group, relative enhancement (RE), D*, and $V_{\text{liver}}/V_{\text{spleen}}$ showed significant differences among the different liver function groups ($P < .001$). Receiver operating characteristic analysis showed that these parameters had the highest area under the curve (AUC) values for distinguishing Child-Pugh A from Child-Pugh B and C groups (0.917, 0.929, and 0.885, respectively). The following liver function model was obtained by multivariate regression analysis: $F(x) = 3.96 - 1.243(\text{RE}) - 0.034(D^*) - 0.080(V_{\text{liver}}/V_{\text{spleen}})$ ($R^2 = 0.811$, $P < .001$). In the patients with cirrhosis, the $F(x)$ of Child-Pugh A, B, and C were 1.16 ± 0.44 , 1.95 ± 0.29 , and 2.79 ± 0.38 , respectively. In the validation group, the AUC for $F(x)$ to distinguish Child-Pugh A from Child-Pugh B and C was 0.973.

CONCLUSION

Combining multiparametric MRI with LV effectively distinguished patients with different Child-Pugh grades. This model could hence be useful as a novel radiological marker to estimate the liver function.

From the Department of Radiology (C.L., J.W., X.L., T.C., R.W., J.Y., Y.Z. ✉ zhyl_003@163.com), The First Affiliated Hospital of Xi'an Jiaotong University, Xi'an, PR China; The Third Hospital of Hebei Medical University (H.L.) Department of Biomedical Engineering (C.L., J.Y.), the Key Laboratory of Biomedical Information Engineering of the Ministry of Education, School of Life Science and Technology, Xi'an Jiaotong University, Xi'an, PR China.

*These authors have contributed equally to this work.

Received 20 January 2022; revision requested 25 February 2022; last revision received 9 June 2022; accepted 2 August 2022.

Publication date: 1 December 2022.

DOI: 10.5152/dir.2022.211325

Liver cirrhosis is a pathological stage characterized by diffuse fibrosis of the liver, formation of pseudo-lobules, and blood vessel proliferation in the liver.¹ Liver function assessment is the main factor affecting the prognosis of patients with liver cirrhosis, and the assessment of preoperative and residual liver function is extremely important for patients with liver cancer.² Moreover, liver function is unevenly distributed in the liver parenchyma and varies between different lobes and segments in cirrhosis.³ The liver morphology changes in different stages of cirrhosis. This change is partly derived from changes in the volume and number of liver parenchymal cells. However, clinical methods for assessing liver function focused on clinical symptoms, biochemical blood parameters, and lack of evaluation of liver morphology.⁴⁻⁶

Magnetic resonance imaging (MRI) can provide morphological and functional information about the liver. Gadoxetic acid disodium (Gd-EOB-DTPA) is a liver-targeting MRI contrast agent which can be specifically ingested by normal hepatocytes.⁷ Images of hepatobiliary phase could accurately assess liver volume (LV) which is another important clinical index for liver function.⁸ Liver function is impaired and the number of hepatocytes with

You may cite this article as: Li C, Liu H, Wang J, et al. Multiparametric MRI combined with liver volume for quantitative evaluation of liver function in patients with cirrhosis. *Diagn Interv Radiol.* 2022;28(6):547-554.

normal Gd-EOB-DTPA uptake is reduced in cirrhosis. At the same time, the uptake of Gd-EOB-DTPA by hepatocytes is reduced due to the proliferation of fibrous stroma and the reduction of organic anion transporter polypeptide (OATP) expression. Consequently, the liver signal decreases during the hepatobiliary phase.⁹ During the progression of cirrhosis, the increased intrahepatic connective tissue reduces hepatic blood flow and diffusion capacity, leading to hepatocyte degeneration, inflammatory infiltration, and fibrosis. All of this leads to changes in liver tissue structure and perfusion. Intravoxel incoherent motion diffusion-weighted imaging (IVIM-DWI) can simultaneously obtain information on liver perfusion and water diffusion. The diffusion coefficient (D) value has high sensitivity and specificity in detecting liver fibrosis.¹⁰ Multiparametric imaging combining conventional techniques could enable a comprehensive examination of the liver.¹¹

In view of the potential value of LV and multiparametric MRI in liver function assessment, this study aims to establish a liver function evaluation model by combining multiparametric MRI with LV and further verify the effectiveness of the model to evaluate liver function.

Methods

This institutional review board–approved (©Ethics Committee of the First Affiliated Hospital of Xi'an Jiaotong University 2016 NO.G-201) retrospective study with waiver of informed consent included 26 normal cases and 101 consecutive cirrhosis patients

who underwent Gd-EOB-DTPA-enhanced MRI and IVIM-DWI. For the modeling group, the data were from patients who underwent abdominal MRI from December 2016 to September 2017. For validating group, the data were from September 2016 to November 2016. The cirrhosis patients were divided into groups A, B, and C according to the Child-Pugh score in both modeling and validating groups.

Inclusion and exclusion criteria for the normal control group

The inclusion criteria for the normal control group were as follows: (i) underwent plain and enhanced 3.0 T MRI; (ii) had no history of drug or alcohol abuse, and no drug therapy 3 months before the examination; (iii) tested negative for hepatitis viruses and had normal laboratory examination of liver function; and (iv) no history of liver surgery. The exclusion criteria for the normal control group were as follows: (i) abnormal liver signs on imaging examination (e.g., diffuse lesions and liver space-occupying lesions) and (ii) poor patient coordination or image artifacts affecting data analysis.

Inclusion and exclusion criteria for the cirrhosis groups

The inclusion criteria for the cirrhosis groups were as follows: (i) underwent plain and enhanced 3.0 T MRI; (ii) history of chronic hepatitis and cirrhosis based on clinical, pathological, and other imaging examinations; (iii) no liver or spleen operation performed before the examination, and no obstructive jaundice; and (iv) Child-Pugh score supported by comprehensive examinations and biochemical laboratory data.

The exclusion criteria for the cirrhosis groups were as follows: (i) poor patient coordination or image artifacts affecting data analysis; (ii) portal vein thrombosis; and (iii) scope of diffuse tumor or focal lesion exceeding the involved liver segment.

MRI protocol

In the modeling group, all cases were examined using a GE Discovery MR750w 3.0 T scanner (General Electric Medical Systems) with a body 16-channel phased-array surface coil. Before upper abdominal scans, the subjects were fasted for 6-8 hours. End-expiratory breath hold training was performed at approximately 1 hour before the examination. Gd-EOB-DTPA (Trade name: Primovist; Bayer Healthcare

AG) at a dose of 0.1 mL/kg was administered. The scanning sequence included conventional T1-weighted image (T1WI) and T2-weighted image (T2WI), 3-phase enhanced scanning (arterial phase, 20 seconds; portal venous phase, 60 seconds; and delayed phase, 120 seconds), IVIM-DWI sequence, and hepatocyte-specific phase scanning (20 minutes after administration of Gd-EOB-DTPA). T1WI plain and enhanced scans were performed using the liver acquisition with volume acceleration sequence with the following parameters: repetition time (TR), 2.8 ms; echo time (TE), 1.3 ms; flip angle (FA), 11; field of view, 400 mm × 420 mm; and slice thickness, 5 mm. T2WI scan was performed using a fat-suppressed fast spin-echo sequence, with the following parameters: TR, 6315.7 ms; TE, 85.3 ms; FA, 90; FOV, 400 mm × 420 mm; and slice thickness, 5 mm. IVIM-DWI was performed using a single-shot spin-echo echo-planar imaging (EPI) sequence after administration of Gd-EOB-DTPA, with b values of 0, 20, 30, 50, 80, 100, 160, 200, 400, 600, and 800 s/mm². The scanning parameters are as follows: TE, 77.4 ms; FA, 90; FOV, 400 mm × 420 mm; slice thickness, 5 mm; number of signal averages, 4; accelerating factor of parallel imaging, 2; respiratory-triggered acquisition with total scan duration, 4.5 minutes. Validation group was collected using a GE Signa HDxt 3.0 T scanner (General Electric Medical Systems). Scanning sequences and parameters were the same as those used for the modeling group, with patients undergoing plain and enhanced abdominal scans.

Image analysis

Gd-EOB-DTPA-enhanced MRI analysis

The data were post-processed using GE AW Functool software. Two radiologists with 7 and 10 years of diagnostic experience in abdominal MRI measured the signal intensity (SI) of the tissues. Regions of interest (ROI) of area about 50-100 mm² were declined on the liver, spleen, and erector spinae on axial images acquired before and 20 minutes after Gd-EOB-DTPA enhancement under a blind condition. Four ROIs were placed on each liver segment at the level of first hepatic hilum. At the same level, 3 ROIs were placed at the spleen and 2 ROIs were placed on the left and right erector spinae (Figure 1). The SI of each ROI was averaged.

$SI_{liver\ pre}$ is the SI of liver before contrast enhancement. $SI_{liver\ post}$, $SI_{spleen\ post}$, and $SI_{muscle\ post}$

Main points

- Among the parameters generated by gadoteric acid disodium-enhanced magnetic resonance imaging (MRI), intravoxel incoherent motion, and liver volume, the relative enhancement (RE), pseudo-diffusion coefficient (D*), and liver-spleen volume ratio (V_{liver}/V_{spleen}) displayed the best liver function classification performance.
- The model F(x) combining multiparametric MRI with liver volume showed an area under the curve of 0.973 in distinguishing Child-Pugh A from Child-Pugh B and C. The sensitivity and specificity were 97.6% and 90.9%, respectively.
- The model integrates the functional and morphological information of the liver. It is useful for quantitative liver function evaluation and is expected to be used for preoperative liver function evaluation.

are the SI of liver, spleen, and muscle 20 minutes after contrast enhancement, respectively. $SI_{liver/spleen}$ is the SI ratio of liver and spleen 20 minutes after contrast enhancement. $SI_{liver/muscle}$ is the SI ratio of liver and erector spinae 20 minutes after contrast enhancement. CEI_{spleen} is the liver enhancement index using spleen as reference. CEI_{muscle} is the liver enhancement index using erector spinae as reference. The formulas for the SI parameters are as follows:

- (1) Relative enhancement (RE) = $(SI_{liver\ post} - SI_{liver\ pre}) / (SI_{liver\ pre})$,
- (2) $SI_{liver/spleen} = SI_{liver\ post} / SI_{spleen\ post}$,
- (3) $SI_{liver/muscle} = SI_{liver\ post} / SI_{muscle\ post}$,
- (4) Contrast-enhanced index (CEI):

$$CEI_{spleen} = (SI_{liver\ post} / SI_{spleen\ post}) / (SI_{liver\ pre} / SI_{spleen\ pre});$$

$$CEI_{muscle} = (SI_{liver\ post} / SI_{muscle\ post}) / (SI_{liver\ pre} / SI_{muscle\ pre}).$$

The SI parameters of the liver, spleen, and erector spinae before and 20 minutes after contrast enhancement were measured again after 1 month by radiologist 1 for intra-observer consistency test.

IVIM-DWI image analysis

IVIM-DWI data were post-processed using GE AW Functool software (AW 4.3, GE Medical System) to generate the pseudo-color maps of the diffusion coefficient (D), pseudo-diffusion coefficient (D*), and perfusion fraction (f) parameters. Four ROIs (area, about 50-100 mm²) were placed on each liver segment at the level of the first hepatic hilum, as close as possible to the level with those of Gd-EOB-DTPA-enhanced analysis. The average value was calculated (Figure 2). Parameter measurements were repeated after 1 month for intra-observer consistency test.

LV image analysis

Image data in Digital imaging and communications in medicine (DICOM) format were imported into the 3-dimensional image generation software, Mimics software (Mimics16.0, Materialise). Three-dimensional solid models of the liver and spleen were obtained by tracing the boundaries of these structures on axial and coronal images. V_{liver} represents the LV, V_{spleen} represents the spleen volume, and V_{liver} / V_{spleen} represents the ratio of the liver and spleen volume (Figure 3). Parameter measurements were repeated after 1 month for intra-observer consistency test.

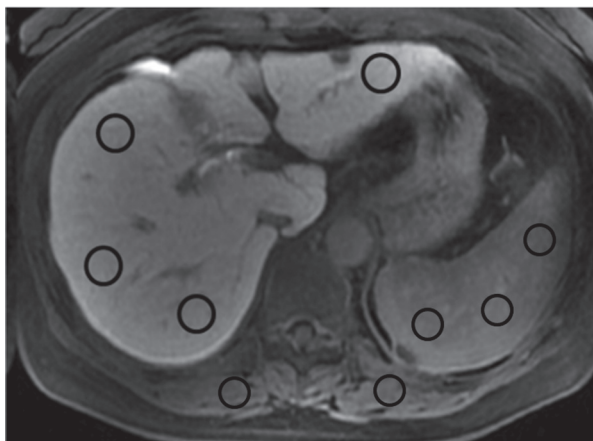


Figure 1. Schematic diagram of ROI placement of liver, spleen, and erector spinae on axial images. ROIs were placed in each liver segment, the spleen, and both sides of the erector spinae at the level of the first hepatic hilum. ROI, regions of interest.

Laboratory examinations

Serum bilirubin, serum albumin, ascites, hepatic encephalopathy, and prothrombin time were collected for Child-Pugh classification into Child-Pugh A (5-6 points), Child-Pugh B (7-9 points), and Child-Pugh C (10-15 points). Laboratory examination was performed within 1 week before or after MRI examination.

Statistical analysis

SPSS 21.0 software (SPSS, Inc.) was used for data analysis. First, an intraclass correlation coefficient (ICC) consistency test

was performed on inter-observer and intra-observer measurements. If the ICC was greater than 0.90, then the reliability was considered excellent, and statistical analysis was performed using the results of the first measurement of radiologist 1. A normal distribution test was performed for all of the data, and a homogeneity test of variances was applied after confirming a normal distribution. One-way analysis of variance was used to analyze the differences in various parameters between different liver function groups, and the Bonferroni test was used for pairwise

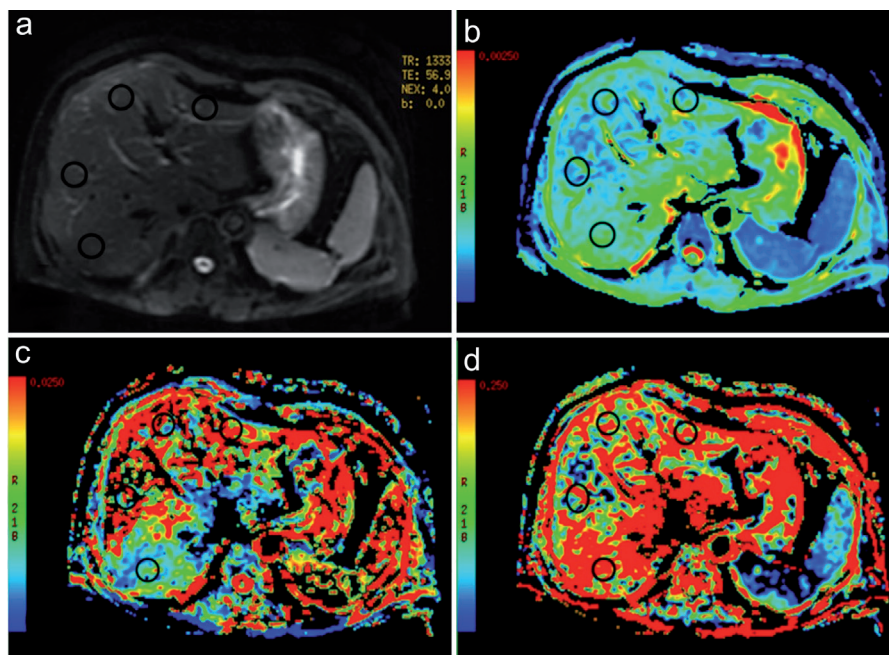


Figure 2. a-d. Schematic diagram of ROI placement of liver IVIM-DWI on the axial image. According to the image of $b = 0$ s/mm² at the first hepatic hilum level, ROIs were placed in each liver segment (a). The ROIs were automatically copied to the pseudo-color maps of D, D*, and f, and the corresponding values were obtained (b-d). D, diffusion coefficient; D*, pseudo-diffusion coefficient; f, perfusion fraction (f); IVIM-DWI, intravoxel incoherent motion diffusion-weighted imaging.

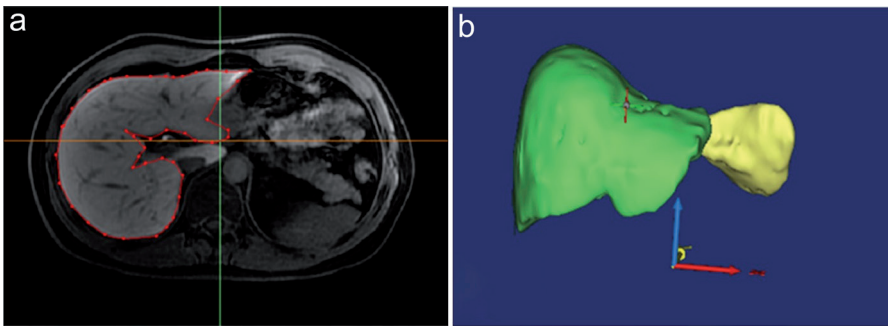


Figure 3. a, b. Schematic diagram of liver volume measurement. By delineating the boundary of liver and spleen on the axial and coronal plane (a), the 3-dimensional solid model and value of liver and spleen were obtained (b).

group comparisons. In cases of heterogeneity of variance, the Kruskal-Wallis rank sum test was used to compare the differences among liver function groups. The receiver operating characteristic (ROC) curves were obtained by MedCalc software (MedCalc 13.0, MedCalc Software Ltd). The parameter with the largest area under the curve (AUC) was selected as effective modeling parameter. These parameters were analyzed by stepwise forward multiple linear regression to establish a multimodal MRI liver function evaluation model. Finally, the model was validated by analyzing the AUC values for liver function of the validation group. Type I error rate: $\alpha = 0.05$.

Results

There were 26 cases in the normal control group, 69 cases with cirrhosis in the modeling group, and 32 cases with cirrhosis in the validation group. The demographic data of each group are shown in Table 1.

The inter-observer and intra-observer ICC of the RE, $SI_{\text{liver/spleen}}$, $SI_{\text{liver/muscle}}$, CEI_{spleen} , and CEI_{liver} were 0.957 (95% CI, 0.942-0.963, $P < .001$) and 0.923 (95% CI, 0.901-0.962, $P = .024$); 0.967 (95% CI, 0.952-0.987, $P < .001$) and 0.990 (95% CI, 0.975-0.996, $P < .001$); 0.974 (95% CI, 0.962-0.981, $P < .001$) and 0.995 (95% CI, 0.988-0.998, $P < .001$); 0.953 (95% CI, 0.949-0.962, $P < .001$) and 0.967 (95% CI,

0.916-0.987, $P < .001$); and 0.942 (95% CI, 0.936-0.951, $P < .001$) and 0.989 (95% CI, 0.973-0.996, $P < .001$), respectively. All the ICCs were greater than 0.90.

Kruskal-Wallis test showed statistically significant differences among different liver function groups (Table 2). Independent-samples Kruskal-Wallis test showed that only RE displayed the statistical difference between all pairwise comparisons (Figure 4a and Appendix). RE gradually decreased with decreasing liver function. The ROC curves revealed that the RE had the largest AUC (0.917) for distinguishing group A from groups B and C (Figure 5a). Therefore, of the parameters related to Gd-EOB-DTPA-enhanced MRI, RE was selected as an effective parameter for liver function evaluation.

The inter-observer and intra-observer ICC of the D, D^* , and f were 0.921 (95% CI, 0.915-0.935, $P < .001$) and 0.935 (95% CI, 0.837-0.974, $P < .001$); 0.961 (95% CI, 0.952-0.973, $P < .001$) and 0.981 (95% CI, 0.953-0.993, $P < .001$); and 0.921 (95% CI, 0.914-0.936, $P < .001$) and 0.943 (95% CI, 0.857-0.978, $P < .001$), respectively. All the ICCs were greater than 0.90.

Kruskal-Wallis test showed statistically significant differences among different liver function groups (Table 2). Independent-samples Kruskal-Wallis test showed that only D^* displayed the statistical difference between all pairwise comparisons (Figure 4b and Appendix). D^* gradually decreased with decreasing liver function. The ROC curves revealed that the D^* had the largest AUC (0.929) for distinguishing group A from groups B and C (Figure 5b). Therefore, of the IVIM-DWI parameters, D^* was selected as an effective parameter for liver function evaluation.

Kruskal-Wallis test showed statistically significant differences among different liver function groups (Table 2). Independent-samples Kruskal-Wallis test showed that only $V_{\text{liver}}/V_{\text{spleen}}$ displayed the statistical difference between all pairwise comparisons (Figure 4c and Appendix). $V_{\text{liver}}/V_{\text{spleen}}$ gradually decreased with decreasing liver function. The ROC curves revealed that the $V_{\text{liver}}/V_{\text{spleen}}$ had the largest AUC (0.885) for distinguishing group A from groups B and C (Figure 5c). Therefore, of the LV parameters, the $V_{\text{liver}}/V_{\text{spleen}}$ was selected as an effective MRI parameter for liver function evaluation.

The RE, D^* , and $V_{\text{liver}}/V_{\text{spleen}}$ were selected as effective parameters for liver function evaluation. The following liver function

Table 1. Clinical data of the normal control cases and cirrhosis patients			
Characteristics	Normal control group	Modeling group	Validation group
Number	26	69	32
Age	53 ± 10	54 ± 10	55 ± 12
Gender			
Male	15	46	22
Female	11	23	10
Liver function classification			
Child-Pugh A		22	13
Child-Pugh B		29	12
Child-Pugh C		18	7
Basic lesion			
Hepatitis B		59	24
Hepatitis C		8	8
Hepatitis B with hepatitis C		2	
Ascites			
With		23	4
Without		46	28
Hepatic encephalopathy			
With		1	0
Without		68	32

Table 2. Kruskal-Wallis test of all the parameters from 3 methods

Parameters	Normal control group	Child-Pugh A group	Child-Pugh B group	Child-Pugh C group	H	P
RE	1.00 (0.85, 1.23)	0.89 (0.60, 1.17)	0.64 (0.60, 0.94)	0.37 (0.23, 0.56)	64.399	<.001**
SI _{liver/spleen}	1.19 (1.03, 1.57)	1.24 (0.99, 1.79)	1.19 (0.90, 1.61)	1.03 (0.66, 1.39)	13.311	.004*
SI _{liver/muscle}	1.18 (0.90, 2.39)	1.12 (0.78, 2.92)	1.06 (0.71, 1.56)	0.92 (0.62, 1.22)	9.368	.025*
CEI _{spleen}	1.15 (0.98, 1.36)	1.13 (1.01, 1.39)	1.02 (0.88, 1.31)	0.94 (0.87, 1.09)	47.511	<.001**
CEI _{muscle}	1.39 (1.18, 1.65)	1.35 (1.12, 1.83)	1.26 (0.96, 1.61)	1.11 (1.00, 1.22)	38.939	<.001**
D	1.13 (0.88, 1.44)	0.97 (0.67, 1.67)	1.14 (0.65, 1.87)	0.82 (0.51, 1.14)	25.700	<.001**
D*	47.95 (36.58, 61.63)	40.61 (28.80, 55.00)	30.52 (23.13, 40.40)	16.63 (6.59, 26.18)	68.187	<.001**
f	31.35 (23.23, 46.69)	32.78 (21.30, 48.05)	24.64 (10.22, 50.88)	25.46 (11.16, 40.18)	15.347	.002*
V _{liver} (cm ³)	1293.52 (1072.76, 1471.21)	1417.24 (806.37, 2042.28)	1303.33 (816.94, 1753.99)	1272.43 (889.55, 1700.41)	2.531	.470
V _{spleen} (cm ³)	235.98 (133.61, 374.21)	543.53 (172.57, 1376.94)	734.97 (313.33, 1301.33)	1193.33 (539.01, 2054.32)	40.672	<.001**
V _{liver} /V _{spleen}	6.05 (3.39, 11.01)	3.02 (1.04, 7.67)	2.57 (0.77, 7.32)	1.33 (0.38, 2.89)	33.861	<.001**

RE, relative enhancement; SI_{liver/spleen}, SI ratio of liver and spleen 20 minutes after contrast enhancement; SI_{liver/muscle}, SI ratio of liver and erector spinae 20 minutes after contrast enhancement; CEI_{spleen}, contrast-enhanced index of spleen as reference; CEI_{muscle}, contrast-enhanced index of muscle as reference; D, diffusion coefficient; D*, pseudo-diffusion coefficient; f, perfusion fraction; V_{liver}, liver volume; V_{spleen}, spleen volume; V_{liver}/V_{spleen}, ratio of the liver and spleen volume.

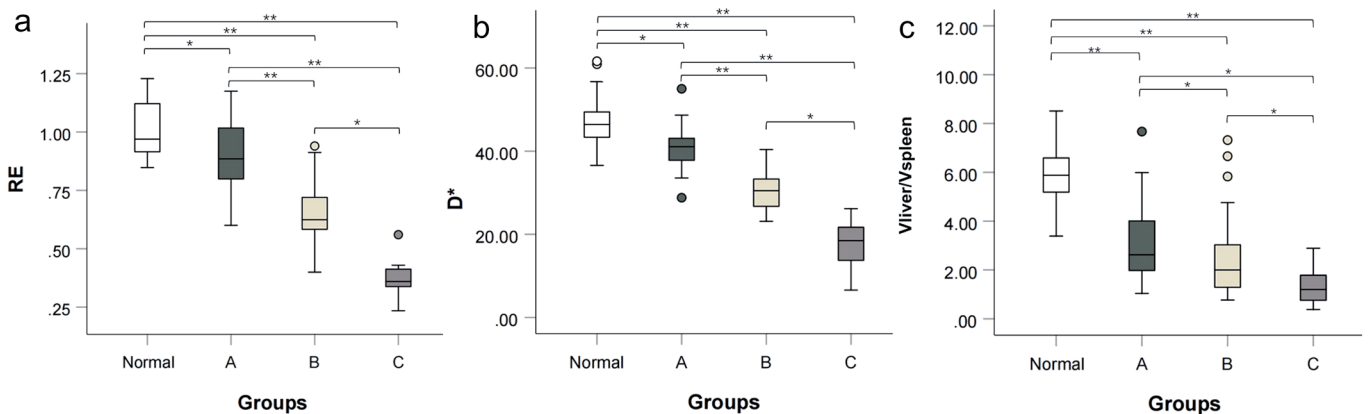


Figure 4. Box plots of RE, D*, and V_{liver}/V_{spleen} in the modeling group. After performing the Kruskal-Wallis test, post hoc tests were done for pairwise comparisons using independent samples Kruskal-Wallis test. All the 3 effective parameters displayed statistical significance in pairwise comparisons (**P* < .05, ***P* < .001). RE, relative enhancement; V_{liver}/V_{spleen}, ratio of the liver and spleen volume.

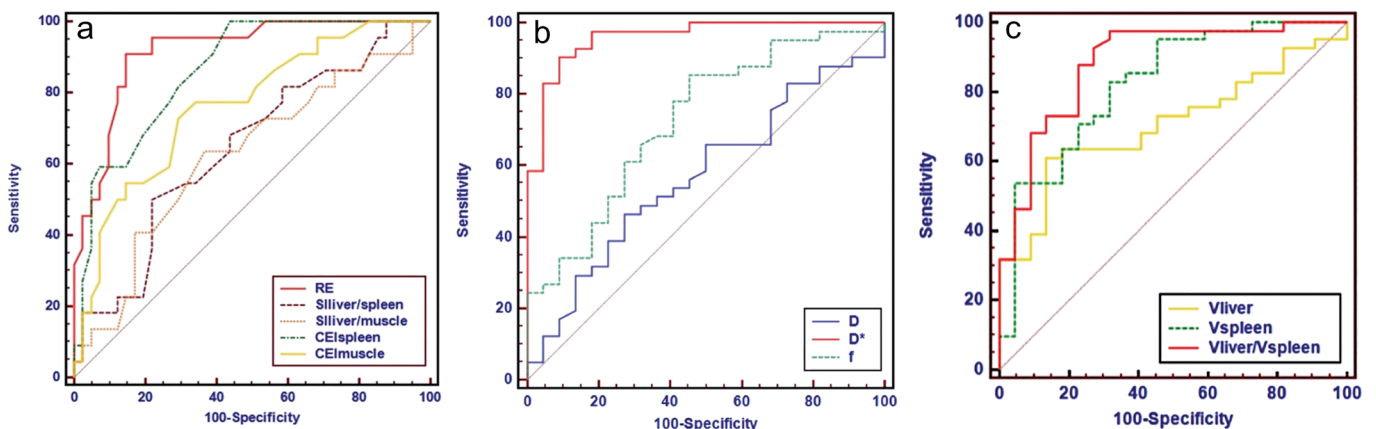


Figure 5. a-c. The ROCs of each parameter from the 3 methods in the modeling group. Diagnostic performance curves of the Gd-EOB-DTPA-enhanced MRI parameters for distinguishing group A from group B and C, in which the RE has the largest AUC (0.917 ± 0.038, 95% CI: 0.849-0.967) (a). Diagnostic performance curves of the IVIM-DWI parameters for distinguishing group A from groups B and C, in which the D* has the largest AUC (0.929 ± 0.034, 95% CI: 0.876-0.978) (b). Diagnostic performance curves of the liver volume parameters for distinguishing group A from groups B and C, in which the V_{liver}/V_{spleen} has the largest AUC (0.885 ± 0.071, 95% CI: 0.778-0.941) (c). AUC, area under the curve; Gd-EOB-DTPA, gadoteric acid disodium; MRI, magnetic resonance imaging; ROC, receiver operating characteristic

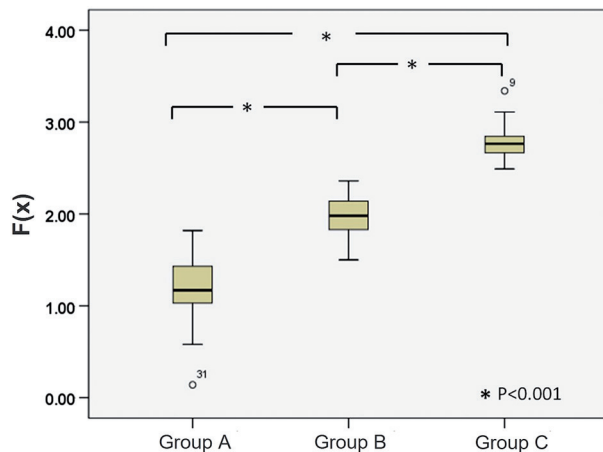


Figure 6. The difference of $F(x)$ among the 3 cirrhosis groups in the modeling group. As liver function declined, the $F(x)$ gradually increased. There were significant statistical differences in $F(x)$ among the 3 groups.

model was obtained by multiple regression analysis: $F(x) = 3.96 - 1.243 (RE) - 0.034 (D^*) - 0.080 (V_{liver}/V_{spleen})$. The $F(x)$ for groups A, B, and C were 1.16 ± 0.44 , 1.95 ± 0.29 , and 2.79 ± 0.38 , respectively, with statistically significant difference among 3 groups (Figure 6). The sensitivity and specificity of the $F(x)$ for distinguishing group A from groups B and C were 95.1% and 95.5%, respectively, with an AUC of 0.986. The AUC of the $F(x)$ was higher than that of the 3 parameters alone (Figure 7).

The RE, D^* , and V_{liver}/V_{spleen} data from the validation group were applied to the evaluation model to obtain corresponding liver function evaluation values. The $F(x)$ for Child-Pugh groups A, B, and C were 1.09 ± 0.43 , 1.94 ± 0.39 , and 2.82 ± 0.48 , respectively, with statistically significant difference among 3 groups ($P < .001$). ROC analysis of the validation group data showed an AUC of 0.973 for the $F(x)$ in distinguishing group A from groups B and C.

The sensitivity and specificity were 97.6% and 90.9%, respectively.

Discussion

In this study, we combined the LV with Gd-EOB-DTPA-enhanced MRI and IVIM-DWI to establish a noninvasive liver assessment model that could simultaneously reflect liver morphology and function. The model showed good efficacy in the validation group, which suggests that the model has potential value in evaluating liver function.

Gd-EOB-DTPA is a liver-targeting MRI contrast agent that is generated by adding lipophilic ethoxy benzyl groups to gadopentetate dimeglumine. It is absorbed into hepatocytes via OATP B1 and B3 on the hepatocyte membrane surface and then excreted into the biliary tract system via multidrug-resistant carrier proteins.¹² The results displayed that the liver signal in the hepatobiliary phase was higher in

normal subjects than in patients with cirrhosis. At the same time, with the decline of liver function, RE decreased significantly. This is consistent with the conclusions of Haimerl et al.¹³ This is because the patient with impaired liver function or advanced liver fibrosis presented with decreased liver parenchymal enhancement after Gd-EOB-DTPA administration. The number of damaged hepatocytes gradually increases with decreased liver function. Moreover, the expression of OATP in the hepatocyte membrane decreases, which reduces Gd-EOB-DTPA absorption by hepatocytes and causes subsequent SI reduction in the liver-specific phase. There is no united standard for SI parameters of GD-EOB-DTPA-enhanced MRI in evaluating liver function, so we selected the following 5 SI parameters based on a review of the literature: RE, $SI_{liver/spleen}$, $SI_{liver/muscle}$, CEI_{spleen} , and CEI_{muscle} . We attempted to select the best parameter from these parameters to evaluate liver function.

The results showed that RE had the highest efficiency. In recent years, increasing evidence has emerged to suggest that RE has a high performance in the assessment of liver function. Wibmer et al¹⁴ found that the RE can effectively predict the risk of liver failure after segmental hepatectomy. Verloh et al¹⁵ analyzed the correlation between RE and liver fibrosis and found that RE could detect and screen early cirrhosis. Poetter Lang et al¹⁶ showed that RE was an independent predictor of fibrosis with high accuracy for the F2 and F4 staging of liver fibrosis. Our finding was consistent with these studies. The efficacy of spleen and erector spinae parameters in liver function evaluation was lower than that of the RE. This may be due to portal hypertension causing splenic venous obstruction and subsequent long-term blood congestion within the spleen. As a result, the spleen signals were more strongly influenced by contrast agent enhancement. The erector spinae have less blood supply and are consequently less affected by contrast agents. However, the erector spinae are located at the edge of the scanning field and are easily affected by coil effects and magnetic field heterogeneity. The CEI has also been used in some studies.¹⁷ Notably, the present study shows that the CEI is less effective than the RE for evaluating liver function. Therefore, the RE was selected as the optimal Gd-EOB-DTPA-enhanced MRI parameter for evaluating liver function.

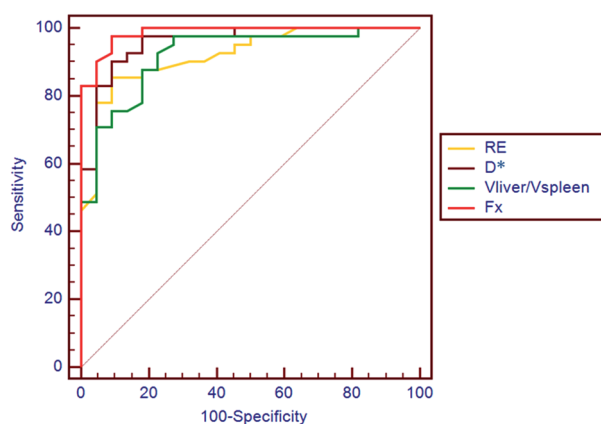


Figure 7. ROC curves of the effective MRI parameters and $F(x)$ for distinguishing group A from groups B and C. The $F(x)$ has the largest AUC (0.986 ± 0.018 , 95% CI: 0.941-0.998). The sensitivity and specificity were 95.1% and 95.5%, respectively.

IVIM-DWI obtained by applying multiple b values can distinguish between simple water molecule diffusion information and microcirculatory perfusion diffusion information within the tissues.¹⁸ With low b values reflecting microvascular tissue perfusion and high b values reflecting water molecule perfusion.^{19,20} IVIM-DWI is a promising method for assessing cirrhosis, where D^* is inversely correlated with interstitial fluid pressure, which affects blood flow and reflects blood perfusion in the capillary network. The D reflects the true diffusion of water molecules. The f reflects tissue capillary richness.²¹ The EPI readout mode of IVIM-DWI is easily affected by magnetic-sensitive artifacts and periodic motions, such as respiration, heartbeats, and gastrointestinal peristalsis, which reduce the image signal-to-noise ratio. Therefore, we tested reproducibility within the same researcher and obtained good reproducibility. The parameter of D^* showed optimal liver function evaluation performance, which was consistent with previous findings.²² This finding may be due to different degrees of collagen fiber deposition, cell necrosis, or apoptosis as well as pseudo-lobule formation during cirrhosis. It leads to hepatic sinusoid stenosis and decreased capillary blood perfusion that result in decreased D^* values.

This study showed that the D and f of the cirrhosis group were lower than those of the normal control group, which was consistent with study of Zhang et al.²³ This finding suggests that hepatic capillary perfusion changes occur before liver structure changes in cirrhosis. In cirrhosis, the decrease of f is presumed to be associated with decreased hepatic vascular volume.²⁴ Interstitial fibrosis causes distortion of the liver parenchyma and vascular structure, slower blood flow, and reduced capillary length.²⁵ The decrease of portal vein blood flow leads to secondary hepatic artery dilatation. Therefore, the f -value associated with vessel volume does not change much.²³ However, D and f were less potent than D^* in discriminating the different liver function groups. Therefore, the D^* was selected as the optimal IVIM-DWI parameter for evaluating liver function. Chen et al.²⁵ reported that the D value was more diagnostic than the D^* value and the f value, probably because the number of b values was less than 200 s/mm² and the choice of study subjects was different.

LV reflects hepatocyte volume as well as liver function to some extent. The liver and spleen are very closely related anatomically, so they also have a certain connection functionally. In this study, $V_{\text{liver}}/V_{\text{spleen}}$ showed the greatest performance in distinguishing three liver function groups. With the aggravation of cirrhosis, the volume of the liver decreases and the volume of the spleen increases. The ratio of liver-to-spleen gradually decreases with decreasing liver function. Therefore, we chose the $V_{\text{liver}}/V_{\text{spleen}}$ as an effective indicator for liver function evaluation. Consistent with our result, Son et al.²⁶ suggest that the $V_{\text{liver}}/V_{\text{spleen}}$ is an important clinical indicator for liver function evaluation.²⁶ Kwon et al. found that the $V_{\text{liver}}/V_{\text{spleen}}$ was less dependent on individual factors than the patient's height, weight, and body surface area. It was superior to LV and spleen volume alone in diagnosing decompensated cirrhosis and detecting portal hypertension.²⁷ This study found that LV increased in group A and decreased in groups B and C, which might be due to compensatory liver responses. In the initial stage of reduced liver function, hepatocytes swell and show a compensatory enlargement. With liver fibrosis progression, liver lobule structure is destroyed and hepatocyte regeneration ability is weakened. Large amounts of collagen fibers are deposited in the extracellular matrix, which results in decreased LV.²⁸

With advances in MRI, there is a growing interest in optimizing and applying functional MRI methods for the assessment of liver function.¹¹ A single functional MRI reflects only one aspect of liver function. Thus, we integrated hepatocyte functional changes, tissue perfusion, and liver morphological changes to derive the multiparametric MRI liver function evaluation model $F(x)$. $F(x)$ showed good performance in assessing liver function compared to Gd-EOB-DTPA-enhanced MRI, IVIM-DWI, and LV alone. Several studies combined multiple functional MRI, LV, and indocyanine green (ICG) laboratory tests to assess liver function in cirrhosis. Our study was consistent with these studies that multiparametric MRI showed advantages in assessing liver function.^{8,29,30} The function of each liver lobe and liver segment is different in liver cirrhosis. However, clinical liver function assessment can only be used to assess overall liver function and cannot reflect differences in local liver function. By measuring the multiparametric MRI of liver lobe

or segment, the corresponding $F(x)$ can be obtained. It is expected to be an indicator of local liver function assessment. However, there is currently no gold standard for evaluating local liver function, and more research is needed to verify the effectiveness of $F(x)$ in evaluating local liver function.

This study has the following limitations. First, the lack of histopathological confirmation in most patients is a major limitation of this study. Liver biopsy is the most objective basis for evaluating the degree of liver cirrhosis. In China, most liver cirrhosis is caused by viral hepatitis. Because of the invasiveness and possible complications of liver biopsy, it is mostly used in patients with cirrhosis of unknown etiology. Nevertheless, this reflected the reality of the clinical routine in the Northwest district of China. Second, the data of the modeling group and the validation group were obtained from different 3.0T MRI scanners. However, the scan parameters of the two scanners were identical, and none of the parameters showed statistical differences between the two groups (Appendix). So, the bias due to different scanners was almost negligible. Third, Child-Pugh classification, which is the most commonly used clinical method for evaluating liver function, was used as a reference standard in this study. Therefore, the evaluation of the degrees of hepatic encephalopathy was influenced by subjective factors. Finally, the Child-Pugh C groups had small sample sizes, which might cause bias. In future studies, the sample size should be increased.

In conclusion, this study established a multiparameter model by combining Gd-EOB-DTPA-enhanced MRI, IVIM-DWI, and LV. The model provides functional and morphological information about the liver. It is useful for quantitative liver function evaluation and is expected to be used for preoperative liver function evaluation.

Conflict of interest disclosure

The authors declared no conflicts of interest.

References

1. Fattovich G, Stroffolini T, Zagni I, Donato F. Hepatocellular carcinoma in cirrhosis: incidence and risk factors. *Gastroenterology*. 2004;127(5):S35-S50. [CrossRef]
2. Kokudo T, Hasegawa K, Shirata C, et al. Assessment of preoperative liver function for surgical decision making in patients with hepatocellular carcinoma. *Liver Cancer*. 2019;8(6):447-456. [CrossRef]

3. Geisel D, Lüdemann L, Hamm B, Denecke T. Imaging-based liver function tests--past, present and future. *ROFO*. 2015;187(10):863-871. [\[CrossRef\]](#)
4. Machicao VI. Model for end-stage liver disease--sodium score: the evolution in the prioritization of liver transplantation. *Clin Liver Dis*. 2017;21(2):275-287. [\[CrossRef\]](#)
5. Gupta S, Chawla Y, Kaur J, et al. Indocyanine green clearance test (using spectrophotometry) and its correlation with model for end stage liver disease (MELD) score in Indian patients with cirrhosis of liver. *Trop Gastroenterol*. 2012;33(2):129-134. [\[CrossRef\]](#)
6. Peng Y, Qi X, Guo X. Child-Pugh versus MELD score for the assessment of prognosis in liver cirrhosis: a systematic review and meta-analysis of observational studies. *Med (Baltim)*. 2016;95(8):e2877. [\[CrossRef\]](#)
7. Van Beers BE, Pastor CM, Hussain HK. Primovist, Eovist: what to expect? *J Hepatol*. 2012; 57(2):421-429. [\[CrossRef\]](#)
8. Chuang YH, Ou HY, Lazo MZ, et al. Predicting post-hepatectomy liver failure by combined volumetric, functional MR image and laboratory analysis. *Liver Int*. 2018;38(5):868-874. [\[CrossRef\]](#)
9. Tsuda N, Matsui O. Cirrhotic rat liver: reference to transporter activity and morphologic changes in bile canaliculi--gadoteric acid-enhanced MR imaging. *Radiology*. 2010;256(3): 767-773. [\[CrossRef\]](#)
10. Fu F, Li X, Chen C, et al. Non-invasive assessment of hepatic fibrosis: comparison of MR elastography to transient elastography and intravoxel incoherent motion diffusion-weighted MRI. *Abdom Radiol (NY)*. 2020;45(1): 73-82. [\[CrossRef\]](#)
11. Zhou IY, Catalano OA, Caravan P. Advances in functional and molecular MRI technologies in chronic liver diseases. *J Hepatol*. 2020;73(5): 1241-1254. [\[CrossRef\]](#)
12. Nassif A, Jia J, Keiser M, et al. Visualization of hepatic uptake transporter function in healthy subjects by using gadoteric acid-enhanced MR imaging. *Radiology*. 2012;264(3):741-750. [\[CrossRef\]](#)
13. Haimerl M, Verloh N, Zeman F, et al. Gd-EOB-DTPA-enhanced MRI for evaluation of liver function: comparison between signal-intensity-based indices and T1 relaxometry. *Sci Rep*. 2017;7:43347. [\[CrossRef\]](#)
14. Wibmer A, Prusa AM, Nolz R, Gruenberger T, Schindl M, Ba-Ssalamah A. Liver failure after major liver resection: risk assessment by using preoperative gadoteric acid-enhanced 3-T MR imaging. *Radiology*. 2013;269(3):777-786. [\[CrossRef\]](#)
15. Verloh N, Probst U, Utpatel K, et al. Influence of hepatic fibrosis and inflammation: correlation between histopathological changes and Gd-EOB-DTPA-enhanced MR imaging. *PLoS One*. 2019;14(5):e0215752. [\[CrossRef\]](#)
16. Poetter-Lang S, Bastati N, Messner A, et al. Quantification of liver function using gadoteric acid-enhanced MRI. *Abdom Radiol (NY)*. 2020;45(11):3532-3544. [\[CrossRef\]](#)
17. Wu WP, Hoi CI, Chen RC, Lin CP, Chou CT. Comparison of the efficacy of Gd-EOB-DTPA-enhanced magnetic resonance imaging and magnetic resonance elastography in the detection and staging of hepatic fibrosis. *Med (Baltim)*. 2017;96(42):e8339. [\[CrossRef\]](#)
18. Zhou Y, Yang G, Gong XQ, et al. A study of the correlations between IVIM-DWI parameters and the histologic differentiation of hepatocellular carcinoma. *Sci Rep*. 2021;11(1):10392. [\[CrossRef\]](#)
19. Le Bihan D, Breton E, Lallemand D, Aubin ML, Vignaud J, Laval-Jeantet M. Separation of diffusion and perfusion in intravoxel incoherent motion MR imaging. *Radiology*. 1988;168(2): 497-505. [\[CrossRef\]](#)
20. LeBihan D. IVIM method measures diffusion and perfusion. *Diagn Imaging (San Franc)*. 1990;12(6):133-136.
21. Mesrobian N, Mürtz P, Sprinkart AM, et al. Comparison of different ROI analysis methods for liver lesion characterization with simplified intravoxel incoherent motion (IVIM). *Sci Rep*. 2021;11(1):22752. [\[CrossRef\]](#)
22. Zhang J, Guo Y, Tan X, et al. MRI-based estimation of liver function by intravoxel incoherent motion diffusion-weighted imaging. *Magn Reson Imaging*. 2016;34(8):1220-1225. [\[CrossRef\]](#)
23. Zhang B, Liang L, Dong Y, et al. Intravoxel incoherent motion MR imaging for staging of hepatic fibrosis. *PLoS One*. 2016;11(1):e0147789. [\[CrossRef\]](#)
24. Li T, Che-Nordin N, Wang YXJ, et al. Intravoxel incoherent motion derived liver perfusion/diffusion readouts can be reliable biomarker for the detection of viral hepatitis B induced liver fibrosis. *Quant Imaging Med Surg*. 2019;9(3): 371-385. [\[CrossRef\]](#)
25. Chen F, Chen YL, Chen TW, et al. Liver lobe based intravoxel incoherent motion diffusion weighted imaging in hepatitis B related cirrhosis: association with Child-Pugh class and esophageal and gastric fundic varices. *Med (Baltim)*. 2020;99(2):e18671. [\[CrossRef\]](#)
26. Son JH, Lee SS, Lee Y, et al. Assessment of liver fibrosis severity using computed tomography-based liver and spleen volumetric indices in patients with chronic liver disease. *Eur Radiol*. 2020;30(6):3486-3496. [\[CrossRef\]](#)
27. Kwon JH, Lee SS, Yoon JS, et al. Liver-to-spleen volume ratio automatically measured on CT predicts decompensation in patients with B viral compensated cirrhosis. *Korean J Radiol*. 2021;22(12):1985-1995. [\[CrossRef\]](#)
28. Lotan E, Raskin SP, Amitai MM, et al. The role of liver segment-to-spleen volume ratio in the staging of hepatic fibrosis in patients with hepatitis C virus infection. *Isr Med Assoc J*. 2017;19(4):251-256.
29. Goshima S, Kanematsu M, Watanabe H, et al. Gd-EOB-DTPA-enhanced MR imaging: prediction of hepatic fibrosis stages using liver contrast enhancement index and liver-to-spleen volumetric ratio. *J Magn Reson Imaging*. 2012; 36(5):1148-1153. [\[CrossRef\]](#)
30. Feier D, Balassy C, Bastati N, Fragner R, Wrba F, Ba-Ssalamah A. The diagnostic efficacy of quantitative liver MR imaging with diffusion-weighted, SWI, and hepato-specific contrast-enhanced sequences in staging liver fibrosis--a multiparametric approach. *Eur Radiol*. 2016; 26(2):539-546. [\[CrossRef\]](#)